Radiative and Auger decay of K-vacancy levels in the Ne, Mg, Si, S, Ar, and Ca isonuclear sequences

P. Palmeri,

Astrophysique et Spectroscopie, Université de Mons-Hainaut, B-7000 Mons, Belgium

patrick.palmeri@umh.ac.be

P. Quinet,

Astrophysique et Spectroscopie, Université de Mons-Hainaut, B-7000 Mons, Belgium and IPNAS, Sart Tilman B15, Université de Liège, B-4000 Liège, Belgium

pascal.quinet@umh.ac.be

C. Mendoza, M. A. Bautista,

Centro de Física, IVIC, Caracas 1020A, Venezuela

claudio@ivic.ve; mbautist@ivic.ve

J. García, and T. R. Kallman

NASA Goddard Space Flight Center, Greenbelt, MD 20771

javier@milkyway.gsfc.nasa.gov; timothy.r.kallman@nasa.gov

ABSTRACT

The HFR and AUTOSTRUCTURE atomic structure codes are used to compute complete data sets of level energies, wavelengths, A-values, and radiative and Auger widths for K-vacancy states of the Ne, Mg, Si, S, Ar, and Ca isonuclear sequences. Ions with electron number $N > 9$ are treated for the first time. Detailed comparisons with previous measurements and theoretical data for ions with $N \leq 9$ are carried out in order to estimate reliable accuracy ratings.

Subject headings: atomic processes — atomic data — line formation — X-rays: general

1. Introduction

While X-ray emission is characteristic of hot ($T \geq 10^6$ K) plasmas, X-ray spectra can also be used to study plasmas of lower ionization via inner-shell transitions. Processes which preferentially remove inner-shell electrons, such as photoionization or collisions with suprathermal particles, can give rise to emission of inner-shell fluorescence lines or K-edge absorption in astrophysical spectra. These features are observed from several important classes of astrophysical sources, being potential diagnostics of their conditions: ionization, gas motions, abundances, and inner-shell ionization rate. The grating instruments on the *Chandra* and *XMM-Newton* space observatories have provided high signal-to-noise spectra of these features, with typical energy resolution of $\varepsilon/\Delta\varepsilon \simeq 500 - 1000$. Exploitation of these diagnostics has been limited by the accuracy of the atomic data for these transitions (energies, cross sections, and lifetimes). This paper is part of a large effort to calculate as many of these data as possible with reliable accuracy using available computational methods. Previous papers in this series have focussed on the data for iron and oxygen; in this and subsequent papers we concentrate on medium-Z elements, namely Ne, Mg, Si, S, Ar, and Ca.

In the X-ray spectra obtained with *Chandra* and *XMM-Newton*, K lines and edges from medium-Z elements have been observed from compact objects in which photoionization is thought to be the dominant ionization mechanism, and from low ionization material which is seen along the line of sight to various bright sources. The active galactic nucleus NGC 3783 observed by Kaspi et al. (2002) shows K-absorption lines of H- and He-like Ne, Mg, Si, S, possibly Ar and Ca, and from lower stages of ionization of Si and S. They are found to be blueshifted and asymmetric, and no correlation is obtained between the velocity shifts and the ionization potential of the ions. Absorption from low and medium stages of Si and S are also seen in the spectra from AGNs MCG-6-30-15 (Lee et al. 2001) and IRAS 13349+2438 (Holczer et al. 2007), and from the X-ray binary Cyg X-1 (Chang & Cui 2007). In emission these lines are seen in the spectra from Vela X-1 by Watanabe et al. (2006) and 4U1700-37 by Boroson et al. (2003). Furthermore, it is likely that future observations, which provide high resolution X-ray spectra from spatially extended sources, will reveal inner-shell features in supernova remnants and stellar coronae. In these sources, such features may indicate existence of non-thermal particles or non-equilibrium ionization, and their analysis requires accurate data for the wavelengths and other atomic quantities associated with the K lines from medium-Z elements.

Following the work by Palmeri et al. (2002, 2003a,b), Bautista et al. (2003, 2004), Mendoza et al. (2004), and Kallman et al. (2004) on the K lines of Fe and by García et al. (2005) on the K-shell photoabsorption of O ions, we report new atomic data for K-vacancy levels in the

Ne, Mg, Si, S, Ar, and Ca isonuclear sequences. Prime objectives are to improve the atomic database of the XSTAR modelling code (Bautista & Kallman 2001) and to prepare ionic targets (configuration expansions and orbitals) for the lengthy computations of the photoabsorption cross sections where both radiative and Auger dampings are key effects. In this respect, available atomic structure data sets—namely K-vacancy level energies, wavelengths, A-values, and Auger widths—for first-row ions with electron number $2 \leq N \leq 10$ are far from complete while for the second row ($11 \leq N \leq 20$) they hardly exist.

Previous work on the K-shell structure of medium-Z elements includes that by Faenov et al. (1994) on the satellites of the He-like resonance line in species with atomic number $12 \leq Z \leq 16$ and electron number $4 \leq N \leq 9$. They have measured wavelengths in a CO_2 laser produced plasma and computed wavelengths, A-values, and Auger rates with the MZ code (Vainshtein & Safronova 1978, 1980). Biémont et al. (2000) have measured wavelengths for Ar ions with $3 \leq N \leq 9$ in a plasma focus discharge, providing also theoretical wavelengths, A-values, and Auger rates calculated with both the HFR atomic structure code (Cowan 1981) and the multiconfiguration Dirac–Fock (MCDF) YODA code of Hagelstein & Jung (1987). K-vacancy level energies, wavelengths, A-values, and Auger and radiative widths have been computed for ions of the beryllium ($6 \leq Z \leq 26$), boron ($6 \leq Z \leq 54$), and carbon ($6 \leq Z \leq 54$) isoelectronic sequences with the MCDF method by Chen (1985), Chen & Crasemann (1988), and Chen et al. (1997), respectively. Inner-shell excitation energies and autoionization rates for ions with $6 \leq Z \leq 54$ and $6 \leq N \leq 9$ have been computed by Safronova & Shlyaptseva (1999) using the $1/Z$ perturbation theory method. Behar & Netzer (2002) have calculated with the relativistic multiconfiguration HULLAC code (Bar-Shalom et al. 2001) wavelengths and oscillator strengths for the 1s-np transitions ($n \leq 3$) in ions of Ne, Mg, Al, Si, S, Ar, and Ca with $2 \leq N \leq 9$. Deslattes et al. (2003) have produced a comprehensive compilation of both measured and theoretical transition energies for K lines and edges in elements with $10 \leq Z \leq 100$. Gorczyca et al. (2003) have audited the fluorescence database by Kaastra & Mewe (1993) which is widely used in modelling codes, in particular their scaling procedures along isoelectronic sequences. The have found serious flaws which appear to compromise the application of this database in plasma modelling.

The outline of the present report is as follows. The numerical methods are briefly described in Section 2 while an analysis of the results based on comparisons with previous experimental and theoretical values is carried out in Section 3. The two supplementary electronic tables are explained in Section 4 while some conclusions are finally discussed in Section 5.

2. Numerical methods

The numerical approach has been fully described by Bautista et al. (2003). The atomic data are computed with the structure codes HFR (Cowan 1981) and AUTOSTRUCTURE (Eissner et al. 1974; Badnell 1986, 1997). Wavefunctions are calculated with the Breit–Pauli relativistic corrections

$$H_{\rm bp} = H_{\rm nr} + H_{\rm 1b} + H_{\rm 2b} \tag{1}$$

where $H_{\rm nr}$ is the usual non-relativistic Hamiltonian. The one-body relativistic operators

$$H_{\rm 1b} = \sum_{n=1}^{N} f_n({\rm mass}) + f_n({\rm d}) + f_n({\rm so}) \tag{2}$$

represent the spin–orbit interaction, f_n(so), and the non-fine-structure mass variation, f_n(mass), and the one-body Darwin correction, f_n(d). The two-body Breit operators are given by

$$H_{\rm 2b} = \sum_{n<m} g_{nm}({\rm so}) + g_{nm}({\rm ss}) + g_{nm}({\rm css}) + g_{nm}({\rm d}) + g_{nm}({\rm oo}) \tag{3}$$

where the fine-structure terms are g_{nm}(so) (spin–other-orbit and mutual spin-orbit) and g_{nm}(ss) (spin–spin), and the non-fine-structure counterparts are g_{nm}(css) (spin–spin contact), g_{nm}(d) (two-body Darwin), and g_{nm}(oo) (orbit–orbit). Core relaxation effects are studied with AUTOSTRUCTURE by comparing ion representations where all the electron configurations have a common basis of orthogonal orbitals, to be referred to hereafter as approximation AS1, with one where each configuration has its own basis, approximation AS2. HFR computes energies, A-values, and Auger rates with bases of non-orthogonal orbitals obtained by optimizing the energy of each configuration, and neglects the part of the Breit interaction (3) that cannot be reduced to a one-body operator. This data set is to be labelled HFR1.

3. Results

We have carried out detailed comparisons with previous data in order to obtain accuracy estimates and detect weak points. In this respect, Palmeri et al. (2006) have already presented the outcome for the S isonuclear sequence. Their comparison with the experimental K-level energies for S XV and S XIV results in differences not larger than 1 eV for HFR1 and 2 eV for AS2, but for the only level reported for S I ([1s]3p^5 ^{3}P$^{\rm o}_2$), differences of 3.3 eV and 3.6 eV are respectively found. The level of agreement between HFR1 and AS2 reported by Palmeri et al. for the S sequence is ∼1 eV for level energies, ∼2 mÅ for wavelengths, and ∼10% for radiative and Auger rates greater than 10^{13} s^{-1}. They cannot explain, however, large discrepancies with the MCDF data by Chen et al. (1997) for C-like

S XI. Since a similar degree of discord with Chen et al. was encountered by Palmeri et al. (2003a) for Fe XXI, we emphasize here comparisons with the experimental and theoretical data sets for Ar ions by Biémont et al. (2000), particularly those computed with the MCDF method, as they will provide more solid evidence on the questionable accuracy of the data by Chen et al.

3.1. Energy levels

With the exception of the He-, Li-, and Be-like species, there is a general lack of experimental K-vacancy level energies for the isonuclear sequences under study here. This severely limits the possibilities of fine-tuning the numerical methods in order to increase data accuracy and to provide reliable rankings. For this reason, we mainly base our approach on computations with the HFR code as it attains marginally more reliable *ab initio* energies due to the use of non-orthogonal basis sets for each electronic configuration.

In Fig. 1 we show the average energy differences between the values listed in the NIST database V3.1.2 (Ralchenko et al. 2007) and HFR1 for the K-vacancy levels in He- and Li-like ions. Differences are never larger than 1 eV if those for Li-like Ar XVI are excluded as the NIST K-vacancy level energies for this ion are believed to be grossly in error. As listed in Table 1, the energy difference for the $1s2s^2\ ^2S_{1/2}$ level in Ar XVI is 0.1 eV while those for the rest are ∼756 eV. The experimental inaccuracies for this ion are further established with the wavelength measurement by Beiersdorfer et al. (2002) for the $1s2s2p\ ^4P^o_{5/2} \rightarrow 1s^22s\ ^2S_{1/2}$ dipole-forbidden transition. They use high-resolution spectroscopy of a low-temperature tokamak plasma to obtain an energy of 3090.25±0.12 eV for the upper level which is in remarkable agreement with the HFR1 value of 3090.1 eV in Table 1. For Be-like Mg and Si the agreement between HFR1 and NIST is well within 2 eV.

Theoretical K-vacancy level energies for ions with $18 \leq Z \leq 26$ and $6 \leq N \leq 9$ are listed by Safronova & Shlyaptseva (1999) which allow a comparison with HFR1 for species with $18 \leq Z \leq 20$. It is found that energy differences are within 3 eV except for the eight levels in both Ar and Ca shown in Table 2. They mainly belong to the O-like type, and the HFR1 values are always larger by as much as 6 eV.

3.2. Wavelengths

Since theoretical wavelengths do not reach spectroscopic accuracy, statistical comparisons with measurements are essential inasmuch as they enable small empirical adjustments

to make the computed values astrophysically useful. It is worth pointing out that, due to the lack of experimental data for ionic species of the second row, this procedure is only currently possible for systems with electron number $N \leq 9$.

Experimental wavelengths for Ar ions with $3 \leq N \leq 9$ have been reported by Biémont et al. (2000) as well as theoretical values computed with the HFR and YODA codes. The two latter data sets are to be hereafter referred to as the HFR2 and MCDF1, respectively. As shown in Fig. 2, a statistical comparison with the measured values can be carried out where the average theory–experiment wavelength difference, $\overline{\Delta\lambda_{\rm e}}$, is plotted as a function of the ion electron number N. It may be seen that theoretical wavelengths appear to be always shorter than the measured values. In the case of our HFR1 data, $|\overline{\Delta\lambda_{\rm e}}|$ increases with N from under 1 mÅ for $N = 3$ to around 6 mÅ for $8 \leq N \leq 9$. A similar behavior is displayed by the MCDF1 values except for $8 \leq N \leq 9$ where $|\overline{\Delta\lambda_{\rm e}}| < 1$ mÅ; this seems to indicate that the transition energies in these two ions have been adjusted with the experimental values. This is certainly also the case with the HFR2 results for $3 \leq N \leq 9$ where $|\overline{\Delta\lambda_{\rm e}}| < 1$ mÅ. However, as shown in Fig. 2, the standard deviations for all three theoretical data sets are around 2–3 mÅ which gives an indication of the level of accuracy that can be attained theoretically.

For the computed MCDF wavelengths listed by Chen & Crasemann (1988) and Chen et al. (1997) for B- and C-like Ar, $|\overline{\Delta\lambda_{\rm e}}| = 2\pm2$ mÅ and $|\overline{\Delta\lambda_{\rm e}}| = 4\pm6$ mÅ, respectively. The somewhat large standard deviation in the C-like system is caused by transitions involving heavily mixed K-vacancy states, in particular $1s(^2S)2s2p^4(^2D)\ ^1D_2$, but the level of agreement is in general similar to that discussed above for HFR1.

Differences between the HFR1 wavelengths and the measurements listed by Faenov et al. (1994) for ions with $12 \leq Z \leq 16$ and $4 \leq N \leq 9$ display a similar behavior to that found in the Ar ions: for each isonuclear sequence, $|\overline{\Delta\lambda_{\rm e}}|$ increases with N. Also, as expected, it decreases with Z along the isoelectronic sequence; for instance, in the case of $N = 9$, $|\overline{\Delta\lambda_{\rm e}}| \approx 18$ mÅ for $Z = 14$ while $|\overline{\Delta\lambda_{\rm e}}| \approx 10$ mÅ for $Z = 16$. On the other hand, we have found three transitions in N-like ions ($N = 7$) with unusually large wavelength differences which are listed in Table 3.

As a result of the comparisons with the spectroscopic data, the HFR1 wavelengths for systems with $3 \leq N \leq 9$ have been empirically shifted with $-\overline{\Delta\lambda_{\rm e}}$.

Behar & Netzer (2002) list wavelengths computed with the HULLAC code for 68 K-transitions arising from the ground level of ions with $2 \leq N \leq 9$. In general, the agreement with HFR1 is better than 10 mÅ and progressively improves with Z up to 3 mÅ for $Z = 20$. As depicted in Table 4, there are however several transitions with noticeable differences, specially for ions with $Z \leq 14$ and $6 \leq N \leq 9$ where the longer HULLAC wavelengths

are probably more accurate than HFR1. Surprisingly large differences (10 mÅ) are found between HULLAC and measurements for transitions in Li-like Ne for which the measured values agree with HFR1 to within 3 mÅ (see Table 4).

HFR1 Kα, Kβ, and edge transition energies for singly ionized species with $10 \leq Z \leq 20$ are compared in Table 5 with the compilation by Deslattes et al. (2003) of experimental and theoretical X-ray transition energies. The HFR1 edge transition energy is estimated using the experimental ionization potential of the neutral and the HFR1 position for the lowest K-vacancy level of the singly ionized stage. The agreement with their theoretical and the experimental Kα transition energies is within 1.5 eV, but discrepancies as large as 7 eV are found with the experimental Kβ values and with the edge energies ($\sim$10 eV) for $12 \leq Z \leq 16$. The soundness of this comparison may be limited by experimental difficulties in assigning weak features and by solid-state effects.

3.3. *A*-values

Present A-values are computed with approximations AS1, AS2, and HFR1. As mentioned in Section 2, in AS2 and HFR1 non-orthogonal orbital bases are used which then account for orbital relaxation in the radiative decay process. It has been found that the 1s orbital is particularly different in valence and K-vacancy states. Since orthogonal bases are used in AS1, a comparison of AS1 and AS2 would give an indication of the importance of this effect.

The radiative data listed by Behar & Netzer (2002) for K transitions, namely f- and A-values, are consistently (10$\pm$5)% below HFR1. To study this situation, we first look at the absorption f-value for the $1s^2\ ^1S_0 \rightarrow 1s2p\ ^1P^o_1$ resonance transition along the He isoelectronic sequence (see Fig. 3). It may be seen that the f-values by Behar & Netzer are about 6% below those by Drake (1979) which are usually taken as the reference. On the other hand, HFR1 is 9% higher and so is AS2 (6%). As shown in Fig. 3, if the HFR1 f-values are recomputed in a single-configuration approximation, the differences with Drake are reduced to 6% and AS1 also does somewhat better (3%). The latter result suggests that perhaps taking into account core relaxation effects does not necessarily lead to improved radiative data. This hypothesis is confirmed by a comparison of available lifetime measurements in He- and Li-like ions with AS1 and AS2 (see Table 6). The computed lifetimes for these $n = 2$ levels are sensitive to the wavefuntions because most of them involve optically forbidden decay channels. Although the agreement of both AS1 and AS2 with experiment is within approximately 10%, it is not clear which is the most accurate. As a conclusion, we are only confident that the accuracy of the HFR1 A-values is at around the 15% level.

This suggested level of accuracy is further supported by a comparison of the HFR1 A-values greater than 10^{13} s^{-1} in Ar ions with those computed by Biémont et al. (2000) in the HFR2 and MCDF1 approximations. In spite of their fine tuning of the transition matrix elements with the experimental energy levels in HFR2, the general agreement is well within 15% except for the few problematic transitions listed in Table 7. It may be seen that for transitions in species with $N = 5$ and $N = 7$, HFR1 and HFR2 are in reasonable agreement in contrast to MCDF1. For $N = 6$, the scatter is large which is surely due to strong admixture of the upper K-vacancy levels produced by the spin-orbit interaction.

A-values calculated by Chen & Crasemann (1988) for B-like Ar using the MCDF method agree within 20% with HFR1 although on average they are ∼10% smaller. However, we find that those computed for C-like Ar by Chen et al. (1997), as shown in Fig. 4, are 37% higher. We also include in this plot the MCDF1 A-values by Biémont et al. (2000) which are within 15% of HFR1 if the problematic values of Table 7 are excluded. Moreover, there are several transitions by Chen et al. that show differences larger than a factor of 2 with HFR1 which have not been taken into account in this comparison.

The comparison of the HFR1 A-values with those calculated by Faenov et al. (1994) using the MZ method for ions with $12 \leq Z \leq 16$ and $4 \leq N \leq 9$ shows a wide scatter: some transitions agree to better than 10% while large discrepancies are found for others.

3.4. Radiative and Auger widths

Auger widths of K-vacancy levels are determined by including all the decay channels $C\epsilon l$, where C are all the $n = 2$ valence configurations of the $(N - 1)$-electron daughter ion and $l \leq 4$.

Biémont et al. (2000) have computed with HFR and the MCDF YODA code Auger widths for K-vacancy states in Ar ions with $3 \leq N \leq 9$ (data sets referred to as HFR2 and MCDF1, respectively). A reasonable agreement (within 20%) with HFR1 is found except for the two levels in the Li-like system ($N = 3$) and the five levels in the Be-like system ($N = 4$) shown in Table 8. Also the MCDF1 K-vacancy levels in the N-like ion ($N = 7$) are on average around 40% larger. The discrepant HFR2 results for the Li-like ion are attributed to typos since a recalculation results in data very similar to the HFR1 values.

MCDF radiative and Auger widths have also been computed for Be-, B-, and C-like Ar by Chen (1985), Chen & Crasemann (1988), and Chen et al. (1997), respectively. For the Be- and B-like systems, they agree with HFR1 to within 10% except for the small Auger widths ($A_a < 10^{12}$ s^{-1}) of the 1s2s2p^2 ^{5}P$_j$ levels in Be-like Ar. For the C-like system, on the

other hand, radiative and Auger widths by Chen et al. are on average larger than HFR1 by 40% and 30%, respectively, with some differences being as large as a factor of 2. Such a poor accord can be appreciated in Fig. 5 where the MCDF1 data by Biémont et al. (2000) is also shown. The latter agrees with HFR1 to within 20%.

The total K-widths quoted by Behar & Netzer (2002) follow a similar trend to that found for their A-values: on average they are found to be about 15% below HFR1, although for some levels large discrepancies are encountered (see Table 9). For such levels, it is shown that the agreement between HFR1 and AS1 is around 5%.

The Auger rates for ions with atomic number $12 \leq Z \leq 16$ and electron number $4 \leq N \leq 9$ computed with the MZ code by Faenov et al. (1994) are found to be in complete disagreement with HFR1.

In their study of the fluorescence database by Kaastra & Mewe (1993), Gorczyca et al. (2003) have computed with AUTOSTRUCTURE configuration-averaged fluorescence yields for the K-vacancy configurations $1s2s^22p$ in Be-like ions and $1s2s^22p^6$ in F-like ions. They also list yields estimated from the MCDF data of Chen (1985) and from the widths computed with HULLAC by Behar & Netzer (2002), the latter having been revised due to missing Auger channels and misquoted widths. In the comparison presented in Table 10, it may be seen that our HFR1 fluorescence yields agree with those by Gorczyca et al. (2003) to within 10% except for the Ne F-like ion (20%). Differences may be due to the non-orthogonal orbital bases and neglect of two-body effects in the HFR code. The agreement between HFR1 and Behar & Netzer (2002) for the Be-like configuration is within 6% but is poorer for the F-like (20%), and that with Chen (1985) for the Be-like ion is better than 15%.

4. Supplementary electronic tables

Computed energy levels, wavelengths, A-values, gf-values, and radiative and Auger widths for ions in the Ne, Mg, Si, S, Ar, and Ca isonuclear sequences can be accessed from the online machine-readable Tables 11[1]–12[2]. The printed samples show data for ions of the Ne isonuclear with electron number $N \leq 3$. It may be seen that in Table 11 levels are identified with the vector $(Z, N, i, 2S+1, L, 2J, \mathrm{Conf})$ where Z is the atomic number, N the electron number, $2S+1$ the spin multiplicity, L the total orbital angular momentum quantum number, J the total angular momentum quantum number, and Conf the level configuration

[1]https://hartree.ivic.ve/tempfiles/tab11.txt

[2]https://hartree.ivic.ve/tempfiles/tab12.txt

assignment. For each level, the spectroscopic energy (when available), the computed HFR1 energy, and its radiative width ($A_{\rm r}$) are listed. For K-vacancy levels, the Auger width ($A_{\rm a}$) and fluorescence yield are additionally given. In Table 12, transitions are identified with the vector (Z, N, k, i) where k and i are the upper and lower level indices, respectively, tabulating its computed wavelength, A-value, and gf-value.

5. Summary and conclusions

Extensive data sets containing energy levels, wavelengths, A-values and radiative and Auger widths for K-vacancy levels in the Ne, Mg, Si, S, Ar, and Ca isonuclear sequences have been computed with the atomic structure codes HFR and AUTOSTRUCTURE which include relativistic corrections. For ionic species of the second row with electron numbers $11 \leq N \leq 20$, it is the first time that such data become available. For first-row ions ($2 \leq N \leq 10$), detailed comparisons have been carried out with available measurements and theoretical values which have brought forth the consistency and accuracy of the present data sets.

Comparisons of the present HFR1 K-vacancy level energies with those listed in the NIST database and with recent measurements support an accuracy rating for ions with electron number $N \leq 4$ of better than 2 eV. Furthermore, we have shown that the NIST energies for K vacancy levels in Li-like Ar are incorrect. Comparisons of the HFR1 wavelengths with the spectroscopic values reported for ions with $N \leq 9$ by Faenov et al. (1994) and Biémont et al. (2000) show that the theoretical wavelengths are consistently shorter. Moreover, along an isonuclear sequence, the average theory–experiment wavelength difference $|\overline{\Delta\lambda}_{\rm e}|$ increases with N. This behavior enables empirical corrections to be made to the HFR1 wavelengths in ions with $N \leq 9$ that are bound to improve accuracy to around 2–3 mÅ. Due to a complete absence of spectroscopic measurements for K transitions in ions of the second row, this fine-tuning procedure cannot be extended at present to species with $N > 9$ whose wavelengths therefore remain uncorrected.

The A-values and Auger widths for the Ar isonuclear sequence previously computed by Biémont et al. (2000) with HFR and the MCDF YODA code have given us the opportunity to benchmark the accuracy of the present data sets. This has been useful to sort out the large discrepancies reported by Palmeri et al. (2003a) for Fe XXI and Palmeri et al. (2006) for S XI with the MCDF data of Chen et al. (1997). Similar discrepancies are found with their data for Ar XIII which, in the light of the good agreement of HFR1 with Biémont et al., are certainly not due to the more formal relativistic representation of the MCDF method. Significant discords of HFR1 with the Auger widths reported by Faenov et al. (1994) for the

Mg, Si, and S isonuclear sequences and with those by Behar & Netzer (2002) for levels in the B and C isoelectronic sequences are difficult to explain. Accuracy ratings of the present A-values and Auger widths greater than 10^{13} s^{-1} are confidently assigned to 15% and 20%, respectively, except for special cases; e.g. transitions involving K-vacancy levels in the carbon isoelectronic sequence where strong admixture causes severe departures.

The present radiative and Auger widths will be used in the computations of the K-shell photoionization cross sections of these medium-Z ions which are required in XSTAR for the modelling of interesting spectral features. Future work will involve extension of the present approach to the Ni isonuclear sequence.

MAB acknowledges partial support from FONACIT, Venezuela, under contract No. S1-20011000912. This work was funded in part by the NASA Astronomy and Physics Research and Analysis Program. Partial support for CM was provided by a travel grant from IVIC and the FNRS of Belgium.

REFERENCES

Armour, I. A., Silver, J. D., & Träbert, E. 1981, J. Phys. B, 14, 3563

Badnell, N. R. 1986, J. Phys. B, 19, 3827

Badnell, N. R. 1997, J. Phys. B, 30, 1

Bar-Shalom, A., Klapisch, M., & Oreg, J. 2001, J. Quant. Spectrosc. Radiat. Transfer, 71, 169

Bautista, M. A., & Kallman, T. R. 2001, ApJS, 134, 139

Bautista, M. A., Mendoza, C., Kallman, T. R., & Palmeri, P. 2003, A&A, 403, 339

Bautista, M. A., Mendoza, C., Kallman, T. R., & Palmeri, P. 2004, A&A, 418, 1171

Behar, E., & Netzer, H. 2002, ApJ, 570, 165

Beiersdorfer, P., Bitter, M., Hey, D., & Reed, K. J. 2002, Phys. Rev. A, 66, 032504

Biémont, E., et al. 2000, Phys. Scr., 61, 555

Boroson, B., Vrtilek, S. D., Kallman, T., & Corcoran, M. 2003, ApJ, 592, 516

Chang, C., & Cui, W. 2007, ApJ, 663, 1207

Chen, M. H. 1985, Phys. Rev. A, 31, 1449

Chen, M. H., & Crasemann, B. 1988, At. Data Nucl. Data Tables, 38, 381

Chen, M. H., Reed, K. J., McWilliams, D. M., Guo, D. S., Barlow, L., Lee, M., & Walker, V. 1997, At. Data Nucl. Data Tables, 65, 289

Cocke, C. L., Curnutte, B., & Randall, R. 1974, Phys. Rev. A, 9, 1823

Cowan, R. D. 1981, The Theory of Atomic Structure and Spectra, (Berkeley, CA: University of California Press)

Crespo López-Urrutia, J. R., Beiersdorfer, P., & Widmann K. 2006, Phys. Rev. A, 74, 012507

Davis, W. A., & Marrus, R. 1977, Phys. Rev. A, 15, 1963

Deslattes, R. D., Kessler, E. G., Indelicato, P., de Billy, L., Lindroth, E., & Anton, J. 2003, Rev. Mod. Phys., 75, 35

Dohmann, H. D. & Mann, R. 1979, Z. Phys. A, 291, 15

Drake, G. W. F. 1979, Phys. Rev. A, 19, 1387

Eissner, W., Jones, M., & Nussbaumer, H. 1974, Comput. Phys., Commun., 8, 270

Faenov, A. Ya., Pikuz, S. A., & Shlyaptseva, A. S. 1994, Phys. Scr., 49, 41

García, J., Mendoza, C., Bautista, M. A., Gorczyca, T. W., Kallman, T. R., & Palmeri, P. 2005, ApJS, 158, 68

Gorczyca, T. W., Kodituwakku, C. N., Korista, K. T., Zatsarinny, O., Badnell, N. R., Behar, E., Chen, M. H., & Savin, D. W. 2003, ApJ, 592, 636

Groeneveld, K. O., Mann, R., Nolte, G., Schumann, S., & Spohr, R. 1975, Phys. Lett. A, 54, 335

Hagelstein, P. L., & Jung, R. K. 1987, At. Data Nucl. Data Tables, 37, 121

Haselton, H. H., Thoe, R. S., Mowat, J. R., Griffin, P. M., Pegg, D. J., & Sellin, I. A. 1975, Phys. Rev. A, 11, 468

Hellmann, H., & Träbert, E. 1985, Nucl. Instr. Meth. Phys. Res. B, 9, 611

Holczer, T., Behar, E., & Kaspi, S. 2007, ApJ, 663, 799

Hubricht, G., & Träbert, E. 1987, Z. Phys. D, 7, 243

Kaastra, J. S., & Mewe, R. 1993, A&AS, 97, 443

Kallman, T. R., Palmeri, P., Bautista, M. A., Mendoza, C., & Krolik, J. H. 2004, ApJS, 155, 675

Kaspi, S., et al. 2002, ApJ, 574, 643

Knystautas, E. J., & Druetta, M. 1985, Phys. Rev. A, 31, 2279

Kramida, A. E., & Buchet-Poulizac, M. -C. 2006, Eur. Phys. J. D, 39, 173

Lee, J. C., et al. 2001, ApJ, 554, L13

Mendoza, C., Kallman, T. R., Bautista, M. A., & Palmeri, P. 2004, A&A, 414, 377

Palmeri, P., Mendoza, C., Bautista, M. A., García, J., & Kallman, T. R. 2006, Rad. Phys. Chem., 75, 1465

Palmeri, P., Mendoza, C., Kallman, T. R., & Bautista, M. A. 2002, ApJ, 577, L119

Palmeri, P., Mendoza, C., Kallman, T. R., & Bautista, M. A. 2003a, A&A, 403, 1175

Palmeri, P., Mendoza, C., Kallman, T. R., Bautista, M. A., & Meléndez, M. 2003b, A&A, 410, 359

Ralchenko, Yu., et al. 2007, NIST Atomic Spectra Database (version 3.1.2), http://physics.nist.gov/asd3, National Institute of Standards and Technology, Gaithersburg, MD

Safronova, U. I., & Shlyaptseva, A. S. 1999, Phys. Scr., 60, 36

Stefanelli, G. S., Beiersdorfer, P., Decaux, V., & Widmann, K. 1995, Phys. Rev. A, 52, 3651

Träbert, E., Beiersdorfer, P., Brown, G. V., Smith, A. J., Utter, S. B., Gu, M. F., & Savin, D. W. 1999, Phys. Rev. A, 60, 2034

Vainshtein, L. A., & Safronova, U. I. 1978, At. Data Nucl. Data Tables, 21, 49

Vainshtein, L. A., & Safronova, U. I. 1980, At. Data Nucl. Data Tables, 25, 311

Varghese, S. L., Cocke, C. L., & Curnutte, B. 1976a, Phys. Rev. A, 14, 1729

Varghese, S. L., Cocke, C. L., Curnutte, B., & Seaman, G. 1976b, J. Phys. B, 9, L387

Watanabe, S., et al. 2006, ApJ, 651, 421

Table 1. K-vacancy level energies (eV) in Ar XVI

Level	Expt[a]	HFR1
$1s2s^2\ ^2S_{1/2}$	3079.0	3079.1
$1s(^2S)2s2p(^3P^o)\ ^4P^o_{1/2}$	3842.3	3086.7
$1s(^2S)2s2p(^3P^o)\ ^4P^o_{3/2}$	3843.8	3087.9
$1s(^2S)2s2p(^3P^o)\ ^4P^o_{5/2}$	3847.1	3090.1
$1s(^2S)2p^2(^3P)\ ^4P_{1/2}$	3876.2	3121.6
$1s(^2S)2p^2(^3P)\ ^4P_{3/2}$	3878.6	3123.0
$1s(^2S)2p^2(^3P)\ ^4P_{5/2}$	3881.0	3124.9
$1s(^2S)2s2p(^1P^o)\ ^2P^o_{1/2}$	3884.8	3124.9
$1s(^2S)2s2p(^1P^o)\ ^2P^o_{3/2}$	3885.9	3125.8
$1s(^2S)2p^2(^1D)\ ^2D_{3/2}$	3896.6	3139.8
$1s(^2S)2p^2(^1D)\ ^2D_{5/2}$	3897.2	3140.4

[a]NIST database V3.1.2 (Ralchenko et al. 2007), T. Shirai et al. (1999, unpublished)

Table 2. K-vacancy level energies (eV) in Ar and Ca

		$Z = 18$		$Z = 20$	
N	Level	HFR1	SS[a]	HFR1	SS[a]
6	$1s2p^5\ ^1P^o_1$	3165.4	3162.0	3935.5	3932.0
7	$1s2p^6\ ^2S_{1/2}$	3157.8	3154.1	3925.7	3921.9
8	$1s2s^22p^5\ ^3P^o_2$	2992.3	2988.4	3734.8	3730.6
8	$1s2s^22p^5\ ^3P^o_1$	2994.0	2990.4	3737.5	3733.8
8	$1s2s^22p^5\ ^3P^o_0$	2995.2	2991.9	3739.4	3736.3
8	$1s2s^22p^5\ ^1P^o_1$	3004.7	3000.5	3749.9	3745.4
8	$1s2s2p^6\ ^3S_1$	3059.8	3054.6	3813.3	3808.0
8	$1s2s2p^6\ ^1S_0$	3076.9	3071.2	3832.9	3827.3

[a]Safronova & Shlyaptseva (1999)

Table 3. HFR1 and experimental wavelengths (Å) with large differences

Z	N	Upper level	Lower level	HFR1	Expt[a]	MZ[a]
14	7	$1s2p^6\ ^2S_{1/2}$	$1s^22s^22p^3\ ^2P^o_{3/2}$	6.6590	7.0156	7.0161
16	7	$1s(^2S)2s2p^5(^3P^o)\ ^4P^o_{1/2}$	$1s^22s2p^4\ ^2D_{3/2}$	5.3141	5.2804	5.2797
	7	$1s2p^6\ ^2S_{1/2}$	$1s^22s^22p^3\ ^2P^o_{3/2}$	5.0434	5.2863	5.2864

[a]Experiment and calculation (MZ code) by Faenov et al. (1994)

Table 4. HFR1 and HULLAC wavelengths (Å) with large differences

Z	N	Upper level	Lower level	HFR1	HULLAC[a]	Expt
10	3	$1s2s2p\ ^2P^o_{1/2}$	$1s^22s\ ^2S_{1/2}$	13.658	13.648	13.655(3)[b]
	3	$1s2s2p\ ^2P^o_{3/2}$	$1s^22s\ ^2S_{1/2}$	13.656	13.646	13.655(3)[b]
	4	$1s2s^22p\ ^1P^o_1$	$1s^22s^2\ ^1S_0$	13.824	13.814	
	6	$1s2s^22p^3\ ^3D^o_1$	$1s^22s^22p^2\ ^3P_0$	14.225	14.239	
	8	$1s2s^22p^5\ ^3P^o_2$	$1s^22s^22p^4\ ^3P_2$	14.490	14.526	
	9	$1s2s^22p^6\ ^2S_{1/2}$	$1s^22s^22p^5\ ^2P^o_{3/2}$	14.596	14.631	
12	6	$1s2s^22p^3\ ^3D^o_1$	$1s^22s^22p^2\ ^3P_0$	9.622	9.631	
	8	$1s2s^22p^5\ ^3P^o_2$	$1s^22s^22p^4\ ^3P_2$	9.797	9.816	
	9	$1s2s^22p^6\ ^2S_{1/2}$	$1s^22s^22p^5\ ^2P^o_{3/2}$	9.875	9.895	9.9129[c]
14	8	$1s2s^22p^5\ ^3P^o_2$	$1s^22s^22p^4\ ^3P_2$	7.052	7.063	7.0665[c]
	9	$1s2s^22p^6\ ^2S_{1/2}$	$1s^22s^22p^5\ ^2P^o_{3/2}$	7.107	7.119	7.1244[c]

[a]Behar & Netzer (2002)

[b]NIST database V3.1.2 (Ralchenko et al. 2007), Kramida & Buchet-Poulizac (2006)

[c]Faenov et al. (1994)

Table 5. Transition energies (eV)

Z	Kα_1	Kα_2	Kβ_1	Kβ_3	Edge
10	849.5	849.4			871.0
	849.2	849.1			870.7
	848.61(26)	848.61(26)	857.89(44)	857.89(44)	870.23(18)
12	1254.6	1254.6	1308.4	1308.4	1311.5
	1254.4	1254.1			1312.3
	1253.688(11)	1253.437(13)	1302.20(40)	1302.20(40)	1303.33(27)
14	1741.2	1741.2	1841.8	1842.8	1849.2
	1741.2	1739.7		1841.8	1850.3
	1739.985(19)	1739.394(34)	1835.96(40)	1835.96(40)	1839.13(37)
16	2309.2	2306.8	2468.7	2470.2	2481.9
	2308.8	2307.0	2467.5	2469.7	2481.7
	2307.885(34)	2306.700(38)	2464.07(14)		2471.63(70)
18	2958.7	2956.6	3192.7	3192.5	3208.4
	2957.9	2955.9	3191.5	3191.3	3207.4
	2957.682(16)	2955.566(16)	3190.49(24)	3190.49(24)	3206.14(54)
20	3692.4	3688.8	4015.3	4015.0	4049.9
	3691.0	3687.6	4014.7	4014.3	4049.4
	3691.719(49)	3688.128(49)	4012.76(38)	4012.76(38)	4050.48(30)

Note. — For each element, the first row lists HFR1 data, the second and third rows respectively give computed and measured values by Deslattes et al. (2003).

Table 6. Lifetimes for He- and Li-like ions

Level	Z	N	τ (ns)		
			AS1	AS2	Expt
1s2s ^{3}S$_1$	10	2	9.10+4	1.01+5	9.17(4)+4[a]
	12	2	1.37+4	1.50+4	1.361(49)+4[b]
	16	2	7.04+2	7.55+2	7.03(4)+2[c]
	18	2	2.11+2	2.24+2	2.03(12)+2[d]
1s2p ^{3}P$^o_0$	18	2	5.11	4.60	4.87(44)[e]
1s2p ^{3}P$^o_1$	12	2	3.26−2	3.07−2	2.90(15)−2[f]
	14	2	7.08−3	6.73−3	6.45(30)−3[f], 6.35(33)−3[g]
	16	2	1.93−3	1.85−3	1.57(18)−3[g]
1s2p ^{3}P$^o_2$	16	2	2.80	2.60	2.5(2)[h]
	18	2	1.58	1.50	1.62(8)[e]
1s2p ^{1}P$^o_1$	14	2	2.59−5	2.52−5	2.9(10)−5[i]
1s2s2p ^{4}P$^o_{5/2}$	10	3	1.09+1	1.01+1	1.04(15)+1[j]
	14	3	2.19	2.07	2.1(1)[k]
	16	3	1.14	1.09	1.1(2)[h]
	18	3	6.33−1	6.08−1	5.94(16)−1[l]
1s2p^2 ^{4}P$_{1/2}$	10	3	5.46−1	4.75−1	5.3(5)−1[m]
	12	3	1.56−1	1.40−1	1.74(17)−1[n]
1s2p^2 ^{4}P$_{3/2}$	10	3	3.90−1	3.46−1	4.0(4)−1[m]
	12	3	9.38−2	8.35−2	9.4(12)−2[n]
1s2p^2 ^{4}P$_{5/2}$	12	3	8.80−3	7.45−3	9(4)−3[n]

[a]Träbert et al. (1999)

[b]Stefanelli et al. (1995)

[c]Crespo López-Urrutia et al. (2006)

[d]Hubricht & Träbert (1987)

[e]Davis & Marrus (1977)

[f]Armour et al. (1981)

[g]Varghese et al. (1976a)

[h]Cocke et al. (1974)

[i]Varghese et al. (1976b)

[j]Groeneveld et al. (1975)

[k]Haselton et al. (1975)

[l]Dohmann & Mann (1979)

[m]Knystautas & Druetta (1985)

[n]Hellmann & Träbert (1985)

Note. — $a \pm b \equiv a \times 10^{\pm b}$.

Table 7. Transitions in Ar ions with questionable A-values (s^{-1})

N	Upper level	Lower level	HFR1	HFR2[a]	MCDF1[a]
5	$1s(^2S)2s2p^3(^3D^o)\ ^4D^o_{3/2}$	$1s^22s2p^2\ ^4P_{3/2}$	1.49+13	1.48+13	1.08+13
	$1s(^2S)2s2p^3(^1D^o)\ ^2D^o_{3/2}$	$1s^22s2p^2\ ^2D_{5/2}$	2.36+13	2.20+13	1.77+13
	$1s(^2S)2s2p^3(^1P^o)\ ^2P^o_{1/2}$	$1s^22s2p^2\ ^2S_{1/2}$	2.62+13	2.97+13	1.72+13
	$1s2p^4\ ^2D_{3/2}$	$1s^22p^3\ ^2P^o_{1/2}$	1.02+13	9.00+12	6.80+12
6	$1s2s^22p^3\ ^3S^o_1$	$1s^22s^22p^2\ ^3P_2$	3.11+13	2.33+13	3.50+13
	$1s(^2S)2s2p^4(^2D)\ ^3D_2$	$1s^22s2p^3\ ^3D^o_2$	7.26+13	1.28+13	2.00+11
	$1s(^2S)2s2p^4(^2D)\ ^3D_2$	$1s^22s2p^3\ ^3D^o_3$	3.45+13	6.29+13	9.60+13
	$1s(^2S)2s2p^4(^2D)\ ^3D_2$	$1s^22s2p^3\ ^3P^o_1$	2.66+11	3.52+13	3.51+13
	$1s(^2S)2s2p^4(^2D)\ ^3D_2$	$1s^22s2p^3\ ^3P^o_2$	3.29+13	4.70+12	1.74+13
	$1s(^2S)2s2p^4(^2D)\ ^3D_1$	$1s^22s2p^3\ ^3P^o_2$	8.07+12	1.12+13	5.80+12
	$1s(^2S)2s2p^4(^4P)\ ^3P_2$	$1s^22s2p^3\ ^3D^o_3$	6.94+13	4.58+13	1.50+13
	$1s(^2S)2s2p^4(^4P)\ ^3P_2$	$1s^22s2p^3\ ^3P^o_2$	7.57+12	3.89+13	2.50+13
	$1s(^2S)2s2p^4(^2D)\ ^1D_2$	$1s^22s2p^3\ ^1P^o_1$	1.01+13	1.45+13	1.79+13
	$1s(^2S)2s2p^4(^2P)\ ^3P_2$	$1s^22s2p^3\ ^1D^o_2$	2.23+13	1.39+13	3.94+13
	$1s(^2S)2s2p^4(^2P)\ ^3P_2$	$1s^22s2p^3\ ^3S^o_1$	2.39+13	3.22+13	1.53+13
	$1s(^2S)2s2p^4(^2P)\ ^3P_2$	$1s^22s2p^3\ ^1P^o_1$	1.29+13	9.30+12	5.50+12
7	$1s(^2S)2s2p^5(^3P^o)\ ^2P^o_{3/2}$	$1s^22s2p^4\ ^2S_{1/2}$	2.67+13	2.72+13	5.30+12
	$1s(^2S)2s2p^5(^3P^o)\ ^2P^o_{1/2}$	$1s^22s2p^4\ ^2D_{3/2}$	1.39+14	1.41+14	2.94+13
	$1s(^2S)2s2p^5(^1P^o)\ ^2P^o_{1/2}$	$1s^22s2p^4\ ^2P_{3/2}$	2.58+13	2.61+13	1.35+14

[a]HFR2 and MCDF1 results computed by Biémont et al. (2000)

Note. — $a \pm b \equiv a \times 10^{\pm b}$.

Table 8. Questionable Auger widths (s^{-1}) for Ar ions

N	Level	HFR1	AS1	HFR2[a]	MCDF1[a]
3	$1s(^2S)2p^2(^3P)\ ^2P_{1/2}$	1.34+11	1.19+11	1.70+12	2.00+11
	$1s(^2S)2p^2(^1S)\ ^2S_{1/2}$	2.41+13	2.15+13	6.39+13	2.21+13
4	$1s2s^22p\ ^1P^o_1$	1.14+14	1.20+14	5.69+13	1.08+14
	$1s(^2S)2s2p^2(^4P)\ ^3P_1$	9.75+13	9.62+13	1.10+14	5.23+13
	$1s(^2S)2s2p^2(^2D)\ ^3D_1$	8.63+13	9.57+13	7.53+13	5.23+13
	$1s(^2S)2s2p^2(^4P)\ ^3P_2$	4.23+13	3.73+13	4.96+13	5.41+13
	$1s2p^3\ ^3S^o_1$	5.06+12	6.23+12	1.90+13	4.50+12

[a]HFR2 and MCDF1 results computed by Biémont et al. (2000)

Note. — $a \pm b \equiv a \times 10^{\pm b}$.

Table 9. Questionable HULLAC K-vacancy level widths (s^{-1})

Z	N	Level	HFR1	AS1	HULLAC[a]
10	5	$1s2s^22p^2\ ^2P_{1/2}$	1.03+14	1.08+14	3.55+13
	6	$1s2s^22p^3\ ^3S^o_1$	1.06+14	1.06+14	5.76+13
	8	$1s2s^22p^5\ ^3P^o_2$	3.71+14	3.71+14	2.55+14
	9	$1s2s^22p^6\ ^2S_{1/2}$	3.92+14	3.88+14	5.80+12
12	5	$1s2s^22p^2\ ^2P_{1/2}$	1.20+14	1.33+14	5.08+13
	6	$1s2s^22p^3\ ^3S^o_1$	1.44+14	1.48+14	7.95+13
14	5	$1s2s^22p^2\ ^2P_{1/2}$	1.63+14	1.67+14	7.58+13
	6	$1s2s^22p^3\ ^3S^o_1$	2.05+14	2.23+14	1.16+14
16	5	$1s2s^22p^2\ ^2P_{1/2}$	2.11+14	2.13+14	1.14+14
	6	$1s2s^22p^3\ ^3S^o_1$	2.80+14	2.95+14	1.70+14
18	5	$1s2s^22p^2\ ^2P_{1/2}$	2.76+14	2.76+14	1.69+14
	6	$1s2s^22p^3\ ^3S^o_1$	3.57+14	3.63+14	2.46+14
20	5	$1s2s^22p^2\ ^2P_{1/2}$	3.61+14	3.59+14	2.47+14
	6	$1s2s^22p^3\ ^3S^o_1$	4.51+14	4.45+14	3.46+14

[a]Widths computed with the HULLAC code by Behar & Netzer (2002)

Note. — The level width is given by the sum of the radiative and Auger widths. Also, $a \pm b \equiv a \times 10^{\pm b}$.

Table 10. Configuration-averaged fluorescence yields

Z	N	Configuration	HFR1	AS3[a]	HULLAC[b]	MCDF[c]
10	4	$1s2s^22p$	0.0223	0.0201	0.0209	0.0191
12			0.0423	0.0393	0.0414	0.0377
14			0.0691	0.0658	0.0685	
16			0.1008	0.0974	0.0984	
18			0.1340	0.1309	0.1273	0.1237
20			0.1673	0.1646	0.1569	
10	9	$1s2s^22p^6$	0.0185	0.0147	0.0215	
12			0.0332	0.0298	0.0380	
14			0.0564	0.0528	0.0630	
16			0.0895	0.0855	0.0983	
18			0.1343	0.1286	0.1443	
20			0.1867	0.1818	0.2001	

[a]Computed with AUTOSTRUCTURE by Gorczyca et al. (2003) including relativistic corrections

[b]Estimated by Gorczyca et al. (2003) from the widths computed with HULLAC by Behar & Netzer (2002) after some revision

[c]Calculated by Gorczyca et al. (2003) from the MCDF data by Chen (1985)

Table 11. Valence and K-vacancy levels for the Ne, Mg, Si, S, Ar, and Ca isonuclear sequences

Z	N	i	$2S+1$	L	$2J$	Level	E(NIST) eV	E(HFR1) eV	$A_{\rm r}(i)$ s^{-1}	$A_{\rm a}(i)$ s^{-1}	Yield
10	1	1	2	0	1	1s 2S1/2	0.0000	0.0000			
10	1	2	2	1	1	2p 2P1/2	1021.4970	1021.4975			
10	1	3	2	0	1	2s 2S1/2	1021.5180	1021.5177			
10	1	4	2	1	3	2p 2P3/2	1021.9530	1021.9528			
10	2	1	1	0	0	1s2 1S0	0.0000	0.0000			
10	2	2	3	0	2	1s2s 3S1	905.0775	904.4935			
10	2	3	3	1	0	1s2p 3Po0	914.7805	914.1721	1.03E+08		
10	2	4	3	1	2	1s2p 3Po1	914.8177	914.2734	3.78E+09		
10	2	5	3	1	4	1s2p 3Po2	915.0099	914.4848	1.14E+08		
10	2	6	1	0	0	1s2s 1S0	915.3360	915.2111	1.54E+02		
10	2	7	1	1	2	1s2p 1Po1	922.0163	921.8277	9.88E+12		
10	3	1	2	0	1	1s22s 2S1/2	0.0000	0.0000			
10	3	2	2	1	1	1s22p 2Po1/2	15.8888	15.8681	5.50E+08		
10	3	3	2	1	3	1s22p 2Po3/2	16.0933	16.0709	5.72E+08		
10	3	4	2	0	1	1s2s2 2S1/2		891.0215	5.31E+11	1.14E+14	0.0046
10	3	5	4	1	1	1s(2S)2s2p(3Po) 4Po1/2		895.1820	2.68E+08	< 5.00E+08	1.0000
10	3	6	4	1	3	1s(2S)2s2p(3Po) 4Po3/2		895.2770	6.86E+08	1.00E+09	0.4069
10	3	7	4	1	5	1s(2S)2s2p(3Po) 4Po5/2		895.4381	5.03E+02	9.59E+07	0.0000
10	3	8	2	1	1	1s(2S)2s2p(3Po) 2Po1/2	908.0482	907.7819	7.98E+12	7.73E+12	0.5080
10	3	9	2	1	3	1s(2S)2s2p(3Po) 2Po3/2	908.0482	907.8962	8.13E+12	6.38E+12	0.5603
10	3	10	4	1	1	1s(2S)2p2(3P) 4P1/2		912.3807	1.76E+09	< 5.00E+08	1.0000
10	3	11	4	1	3	1s(2S)2p2(3P) 4P3/2		912.4757	1.98E+09	6.00E+09	0.2481
10	3	12	4	1	5	1s(2S)2p2(3P) 4P5/2		912.6306	2.39E+09	3.70E+10	0.0607
10	3	13	2	1	1	1s(2S)2s2p(1Po) 2Po1/2		914.3583	9.06E+11	7.57E+13	0.0118
10	3	14	2	1	3	1s(2S)2s2p(1Po) 2Po3/2		914.4365	7.55E+11	7.70E+13	0.0097
10	3	15	2	2	3	1s(2S)2p2(1D) 2D3/2	920.4218	920.5238	4.25E+12	1.29E+14	0.0319
10	3	16	2	2	5	1s(2S)2p2(1D) 2D5/2	920.4218	920.5326	4.22E+12	1.30E+14	0.0314
10	3	17	2	1	1	1s(2S)2p2(3P) 2P1/2		922.5025	1.32E+13	2.00E+09	0.9998
10	3	18	2	1	3	1s(2S)2p2(3P) 2P3/2		922.6991	1.32E+13	4.05E+11	0.9702
10	3	19	2	0	1	1s(2S)2p2(1S) 2S1/2		932.4598	3.95E+12	1.92E+13	0.1706

Note. — The complete version of this table is in the electronic edition of the Journal. The printed edition contains only a sample.

Table 12. K-vacancy transitions in the Ne, Mg, Si, S, Ar, and Ca isonuclear sequences

Z	N	k	i	λ 0.1 nm	$A(k,i)$ s^{-1}	$gf(i,k)$
10	2	4	1	13.5582	3.67E+09	3.04E−04
10	2	7	1	13.4470	9.87E+12	8.04E−01
10	3	4	2	14.1641	1.80E+11	1.09E−02
10	3	4	3	14.1673	3.49E+11	2.10E−02
10	3	5	1	13.8471	2.69E+08	1.54E−05
10	3	6	1	13.8456	6.86E+08	7.88E−05
10	3	8	1	13.6548	7.98E+12	4.46E−01
10	3	9	1	13.6531	8.13E+12	9.09E−01
10	3	10	2	13.8265	5.31E+08	3.05E−05
10	3	10	3	13.8297	2.22E+07	1.28E−06
10	3	11	2	13.8251	5.52E+06	6.34E−07
10	3	11	3	13.8282	7.60E+08	8.72E−05
10	3	12	3	13.8258	1.15E+09	1.99E−04
10	3	13	1	13.5566	9.00E+11	4.96E−02
10	3	14	1	13.5554	7.49E+11	8.26E−02
10	3	15	2	13.7020	3.82E+12	4.31E−01
10	3	15	3	13.7051	4.25E+11	4.79E−02
10	3	16	3	13.7050	4.22E+12	7.13E−01
10	3	17	2	13.6721	8.92E+12	5.00E−01
10	3	17	3	13.6752	4.32E+12	2.42E−01
10	3	18	2	13.6692	1.90E+12	2.13E−01
10	3	18	3	13.6722	1.13E+13	1.27E+00
10	3	19	2	13.5236	1.21E+12	6.67E−02
10	3	19	3	13.5266	2.73E+12	1.50E−01

Note. — The complete version of this table is in the electronic edition of the Journal. The printed

edition contains only a sample.

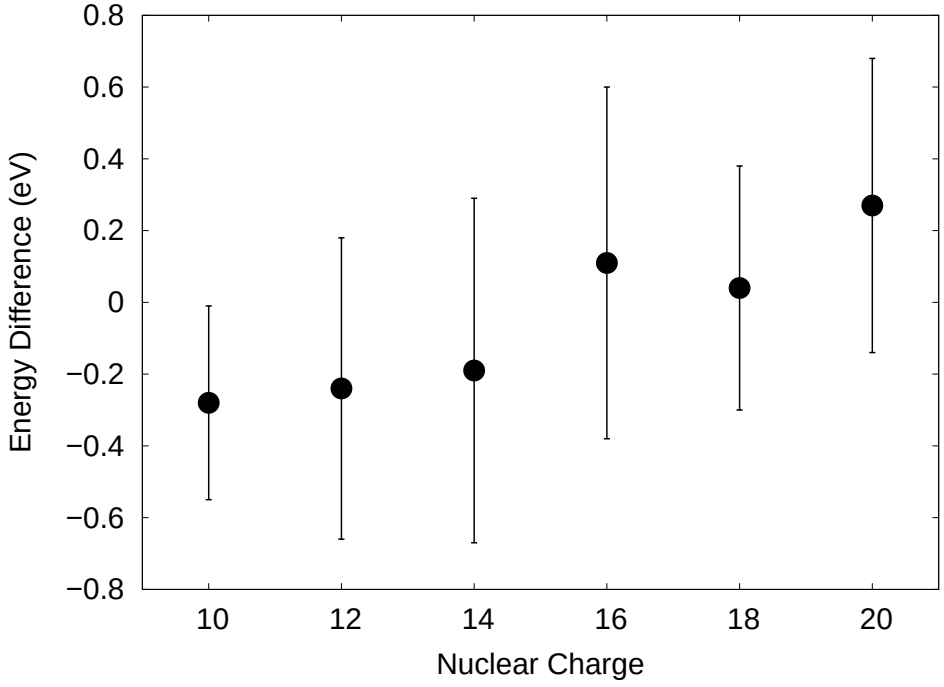

Fig. 1.— Average differences between the HFR1 energies and those in the NIST database V3.1.2 (Ralchenko et al. 2007) for the K-vacancy levels in the He and Li isoelectronic sequences. Error bars indicate the standard deviation. For nuclear charge $Z = 18$, the experimental level energies for the Li-like ion have been excluded as they are believed to be incorrect.

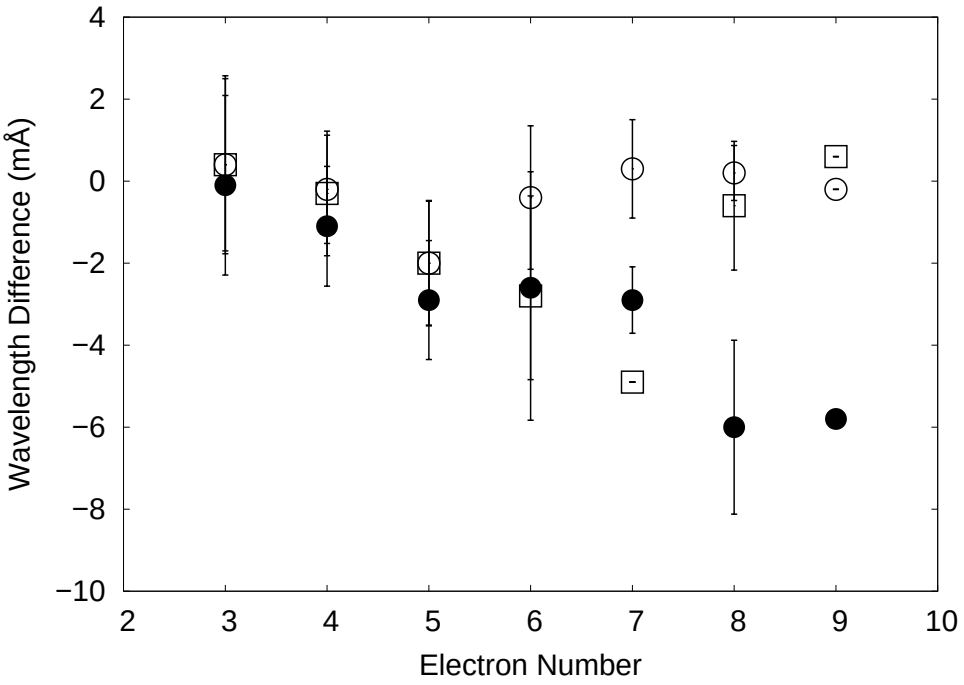

Fig. 2.— Average wavelength difference $\overline{\Delta\lambda_{\rm e}}$ (mÅ) as a function of the electron number for ions in the Ar isonuclear sequence. $\overline{\Delta\lambda_{\rm e}}$ is determined with respect to the spectroscopic values of Biémont et al. (2000). Filled circles: HFR1 values. Circles: HFR2 results by Biémont et al. (2000). Squares: MCDF1 results by Biémont et al. (2000). A large error bar for the MCDF1 value at $N = 7$ has been removed for clarity.

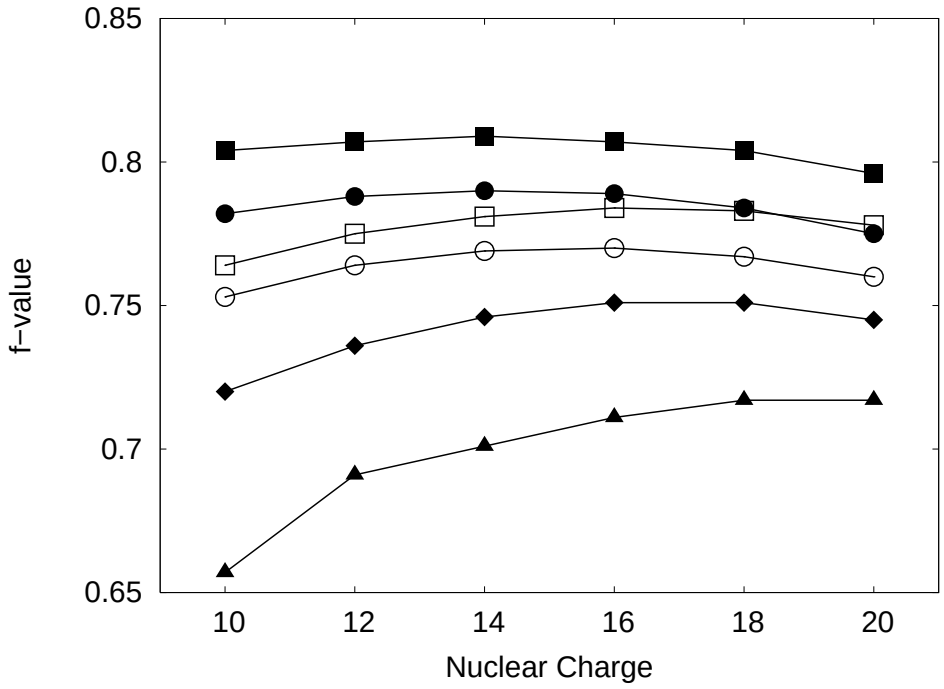

Fig. 3.— Absorption f-value for the $1s^2\ {}^1S_0 \rightarrow 1s2p\ {}^1P^o_1$ resonance transition in the He isoelectronic sequence. Filled squares: HFR1. Filled cirles: AS2. Circles: AS1. Squares: HFR, single configuration. Filled diamonds: values by Drake (1979) calculated in a unified relativistic theory. Filled triangles: data computed with the HULLAC code by Behar & Netzer (2002).

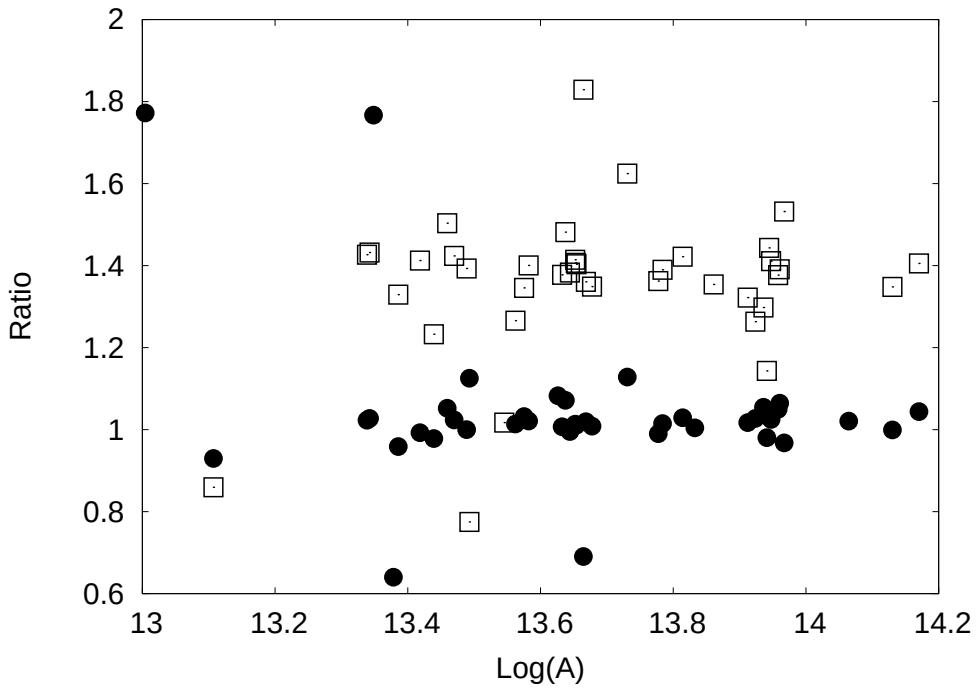

Fig. 4.— Comparison of the present HFR1 A-values for K transitions in C-like Ar with two independent MCDF calculations. Squares: Chen et al. (1997). Filled circles: MCDF1 A-values by Biémont et al. (2000). It is found that the data by Chen et al. (1997) are on average larger by 37% with respect to HFR1.

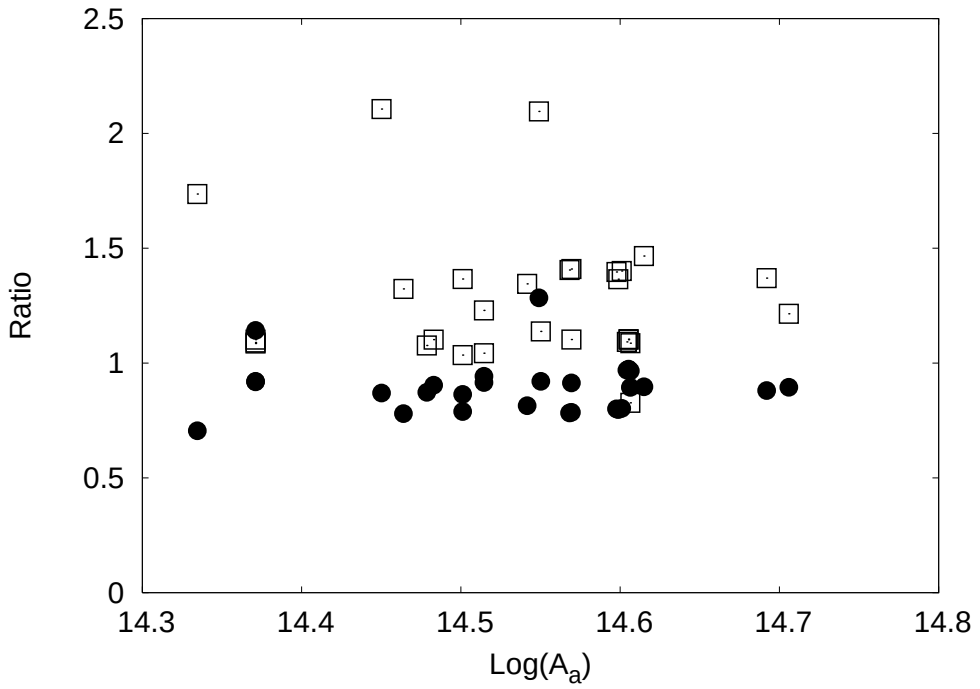

Fig. 5.— Comparison of the present HFR1 Auger widths for K-vacancy levels in C-like Ar with two independent MCDF calculations. Squares: Chen et al. (1997). Filled circles: MCDF1 Auger widths by Biémont et al. (2000). It is found that the data by Chen et al. (1997) are on average larger by 30%.